# Autonomous Four-Dimensional Mapping and Tracking of a Coastal Upwelling Front by an Autonomous Underwater Vehicle

**Yanwu Zhang**
*Monterey Bay Aquarium Research Institute, 7700 Sandholdt Road, Moss Landing, California 95039*
**James G. Bellingham**
*Woods Hole Oceanographic Institution, 266 Woods Hole Road, MS #10, Woods Hole, Massachusetts 02543*
**John P. Ryan, Brian Kieft, and M. Jordan Stanway**
*Monterey Bay Aquarium Research Institute, 7700 Sandholdt Road, Moss Landing, California 95039*

Received 26 August 2014; accepted 29 May 2015

Coastal upwelling is a wind-driven ocean process that brings cooler, saltier, and nutrient-rich deep water upward to the surface. The boundary between the upwelling water and the normally stratified water is called the "upwelling front." Upwelling fronts support enriched phytoplankton and zooplankton populations, thus they have great influences on ocean ecosystems. Traditional ship-based methods for detecting and sampling ocean fronts are often laborious and very difficult, and long-term tracking of such dynamic features is practically impossible. In our prior work, we developed a method of using an autonomous underwater vehicle (AUV) to autonomously detect an upwelling front and track the front's movement on a fixed latitude, and we applied the method in scientific experiments. In this paper, we present an extension of the method. Each time the AUV crosses and detects the front, the vehicle makes a turn at an oblique angle to recross the front, thus zigzagging through the front to map the frontal zone. The AUV's zigzag tracks alternate in northward and southward sweeps, so as to track the front as it moves over time. This way, the AUV maps and tracks the front in four dimensions—vertical, cross-front, along-front, and time. From May 29 to June 4, 2013, the Tethys long-range AUV ran the algorithm to map and track an upwelling front in Monterey Bay, CA, over five and one-half days. The tracking revealed spatial and temporal variabilities of the upwelling front. 

## 1. INTRODUCTION

Marked by enhanced horizontal gradients in water properties, fronts develop in the sea across a vast range of spatial and temporal scales (Belkin, Cornillon, & Sherman, 2009), and they are associated with enhanced turbulence and energy dissipation (D'Asaro, Lee, Rainville, Harcourt, & Thomas, 2011). Coastal upwelling is a wind-driven ocean process that brings cooler, saltier, and usually nutrient-rich deep water upward, replacing warmer, fresher, and nutrient-depleted surface water, as illustrated in the left panel of Figure 1. In addition to enrichment of primary production from upwelled nutrients (Barber & Smith, 1981), upwelling generates dynamic fronts that influence marine ecology in a variety of ways. In the major eastern boundary upwelling systems of the northeastern and southeastern Atlantic and Pacific, the creation of fronts occurs frequently (Smith, 1981).

Direct correspondence to: Yanwu Zhang, e-mail: yzhang@mbari.org

Our study region, Monterey Bay, California, lies in the eastern boundary upwelling system of the North Pacific. When a northwesterly wind persists in spring and summer along the coastline, intense upwelling develops at Point Año Nuevo, and the cold upwelling filaments spread southeastward across the mouth of the bay, as shown in the satellite sea surface temperature (SST) image in the middle panel of Figure 1. In the northern bay, however, the water column typically remains stratified (warm at surface and cold at depth) because that region is sheltered from upwelling-inducing wind by the Santa Cruz mountains, and it is sheltered from the upwelling filaments by the coastal recess. Flow convergence develops at the boundary between the upwelling filaments and the stratified northern bay water, forming the "upwelling front" (Ryan, McManus, & Sullivan, 2010). At this convergent boundary, motile phytoplankton can accumulate through biological-physical interactions (Ryan et al., 2009, 2010). For certain types of phytoplankton, this accumulation can result in harm to marine life (Jessup et al., 2009). Vertical shear in the front can

Journal of Field Robotics 33(1), 67–81 (2016) 
View this article online at wileyonlinelibrary.com • DOI: 10.1002/rob.21617

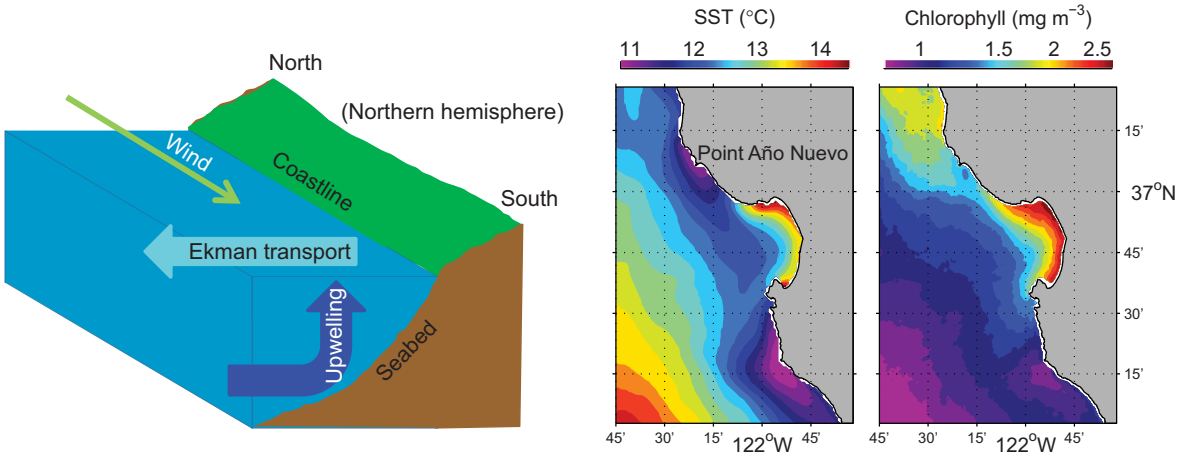


**Figure 1.** Left panel: wind-driven coastal upwelling. Middle and right panels: SST and sea surface chlorophyll level in June (averaged from 2004 to 2008) in Monterey Bay.

create very thin layers of phytoplankton (Ryan, McManus, Paduan, & Chavez, 2008).

Zooplankton can also accumulate at the upwelling front (Harvey et al., 2012; Ryan, Harvey, Zhang, & Woodson, 2014). Larval accumulation and transport within upwelling fronts has been found to organize recruitment patterns of species that populate intertidal and coastal reef habitats (Woodson et al., 2009, 2012). While spatial coincidence between fronts and recruitment hotspots along the coast has been documented, direct observation of frontal ecology has been very limited. In addition to local physical-biological interactions, upwelling fronts can generate internal waves that propagate to affect marine ecology far from the front (Woodson et al., 2011).

Upwelling fronts move due to variations of wind and ocean circulation, as shown in Figure 2. Detection and tracking of an upwelling front is important for investigating the formation and evolution of the upwelling process, and it enables targeted sampling of the different water types across the front. Traditional ship-based methods for detecting and sampling fronts are often laborious and very difficult, and long-term tracking is practically impossible. Existing front-detection methods based on satellite SST (Belkin, Cornillon, & Sherman, 2009; Belkin & O'Reilly, 2009; Ullman & Cornillon, 2000) only use temperature at the sea surface, and they are designed for data postprocessing but not for real-time front detection. The importance and the challenges of studying dynamic fronts motivate advancements in autonomous methods of frontal mapping and tracking to more effectively capture the spatial and temporal variability of these complex phenomena.

In our prior work, we developed a real-time algorithm for an autonomous underwater vehicle (AUV) to autonomously identify an upwelling front, map the water columns across the front, and track the front's movement (Zhang, Godin, Bellingham, & Ryan, 2012a; Zhang, Ryan, Bellingham, Harvey, & McEwen, 2012b). This algorithm is based on the vertical temperature structure measured on the AUV's sawtooth (i.e., yo-yo) trajectory. In stratified water, the vertical temperature difference is large: warm at surface and cold at depth. The upwelling process breaks down stratification and makes water properties more homogeneous over depth. Consequently, the vertical temperature difference between shallow and deep depths is small in upwelling water. The distinct vertical temperature structures of stratified water and upwelling water are illustrated in the color panel in Figure 3. To enable an AUV to autonomously differentiate between upwelling and stratified water columns, we established a key classification metric—the vertical temperature difference between shallow and deep depths (Zhang et al., 2011), which was subsequently modified as the vertical temperature homogeneity index (VTHI), defined as follows (Zhang et al., 2012b):

$$\Delta Temp_{vert} = \frac{1}{N}\Sigma_{i=1}^{N}|Temp_{depth\_i} - \frac{1}{N}\Sigma_{i=1}^{N}Temp_{depth\_i}|, \quad (1)$$

where $i$ is the depth index, and $N$ is the total number of depths included for calculating $\Delta Temp_{vert}$. $Temp_{depth\_i}$ is the temperature at the $i$th depth. $\frac{1}{N}\Sigma_{i=1}^{N}Temp_{depth\_i}$ is the average temperature of those depths. $|Temp_{depth\_i} - \frac{1}{N}\Sigma_{i=1}^{N}Temp_{depth\_i}|$ measures the difference (absolute value) between the temperature at each individual depth and the depth-averaged temperature. The average difference $\Delta Temp_{vert}$ (averaged over all participating depths) is a measure of the vertical homogeneity of temperature in the water column, which is significantly smaller in upwelling water than in stratified water.

Suppose an AUV flies from stratified water to upwelling water on a yo-yo trajectory (in the vertical dimension). Figure 3 illustrates the algorithm for the AUV to

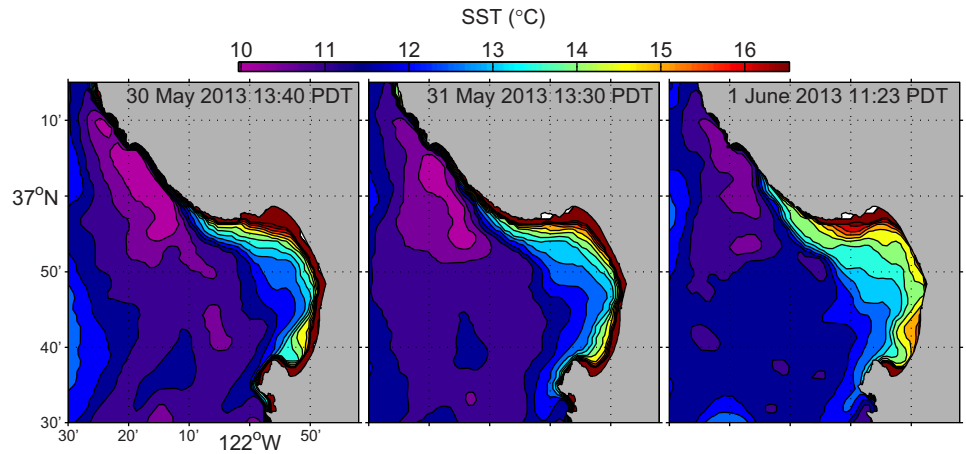


**Figure 2.** Satellite SST in Monterey Bay shows the upwelling front's movement over three days (during the AUV front-tracking experiment to be presented in Section 4).

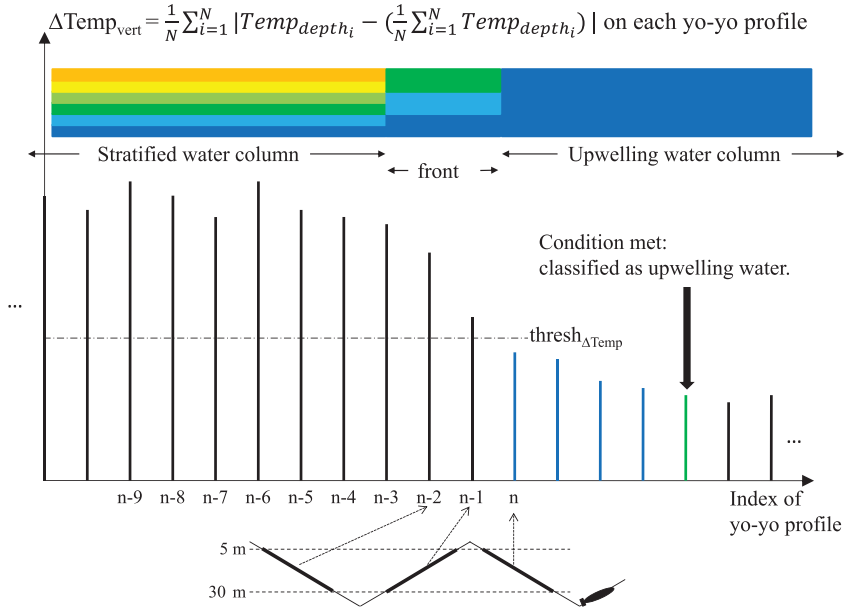


**Figure 3.** Illustration of the AUV's algorithm for determining that it has departed from a stratified water column and entered an upwelling water column. The distinct vertical temperature structures in stratified and upwelling water columns are illustrated in the color panel (temperature from high to low is represented by color ranging from orange to blue).

determine that it has departed from the stratified water column and entered the upwelling water column. On each yo-yo profile (descent or ascent), the AUV records temperatures at the participating depths to calculate $\Delta Temp_{vert}$ in real time. When $\Delta Temp_{vert}$ falls below a threshold $thresh_{\Delta Temp}$ for a number of consecutive yo-yo profiles, the AUV determines that it has entered the upwelling water column. Conversely, suppose the AUV flies from upwelling water to stratified water on a yo-yo trajectory. When $\Delta Temp_{vert}$ rises above $thresh_{\Delta Temp}$ for a number of consecutive yo-yo profiles, the AUV determines that it has entered the stratified water column. To avoid false detection due to measurement noise or existence of isolated water patches, the algorithm only sets the detection flag when $\Delta Temp_{vert}$ meets the threshold for a number of consecutive yo-yo profiles.

In our initial front-tracking algorithm, on each east-west AUV transect, the vehicle detects the front, continues flight for some distance (to sufficiently cover the frontal zone), and then reverses course. The AUV repeats this action to effectively track the front on a fixed latitude. In two

experiments in Monterey Bay in 2011 and 2012, MBARI's Tethys AUV successfully ran this algorithm to track upwelling fronts over several days (Zhang et al., 2012a; Zhang, Ryan, Godin, & Bellingham, 2012c). However, because the front tracking was confined to the cross-front dimension on a fixed latitude, it could not reveal the along-front shape and its temporal variation. To obtain a full picture of a meandering upwelling front, we need to extend the method to also cover the along-front dimension.

## 2. ALGORITHM FOR 4D TRACKING OF AN UPWELLING FRONT

Building upon our previous work, we have developed a method of using an AUV to map and track an upwelling front in four dimensions—vertical, cross-front, along-front, and time. The method was presented in a conference paper (Zhang, Bellingham, Ryan, Kieft, & Stanway, 2013) ("Two-Dimensional" in the title did not count the dimensions of depth and time), but the experimental results reported therein were preliminary. In this paper, the method and experiment design are fully described, and a complete analysis of the experimental data is presented.

### 2.1. Front-tracking Steps

One key element in the new method is that the AUV makes turns at an oblique angle (rather than reversing course) after detecting the front. This way, the vehicle zigzags through the front to map it and track it. The AUV's zigzag tracks alternate in northward and southward sweeps, so as to track the front as it moves over time, as illustrated in Figure 4. The new method comprises the following steps:

- The AUV starts the missions, say, from stratified water (where $\Delta Temp_{vert}$ is high), flying toward upwelling water (where $\Delta Temp_{vert}$ is low), on a yo-yo trajectory between surface and depth that is sufficiently deep for showing the contrast between the two distinct water columns. When $\Delta Temp_{vert}$ falls below $thresh_{\Delta Temp}$ for a number of consecutive yo-yo profiles, the AUV determines that it has passed the front and entered the upwelling water column.
- The AUV continues flight in the upwelling water for some distance to sufficiently cover the frontal zone, and then turns an oblique angle to fly back to the stratified water. For the AUV to effectively track the front, we set the oblique turning angle to a value so that the vehicle intersects the front at a close-to-normal angle. (If the AUV's heading is at a small angle to the front or even parallel to it, the vehicle risks losing track of the front.)
- On the way back to the stratified water, when $\Delta Temp_{vert}$ rises above $thresh_{\Delta Temp}$ for a number of consecutive yo-yo profiles, the AUV determines that it has passed the front and entered the stratified water column.

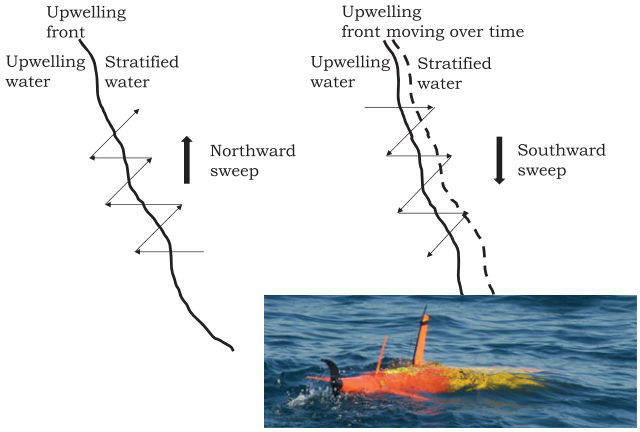


**Figure 4.** Illustration of the AUV's horizontal tracks during 4D front-tracking. The AUV's zigzag tracks alternate in northward and southward sweeps between a northern bound and a southern bound. Over the duration of the sweeps, the front has moved from the dashed curve to the solid curve (right panel). The photo shows the Tethys AUV (Bellingham et al., 2010b) deployed in Monterey Bay. The orange tail section of the vehicle is the propulsion and control section, which also includes antennae for Iridium and Argos satellites, GPS, and line-of-sight radio-frequency communications. The yellow center section is the main pressure vessel housing vehicle electronics and batteries. The orange head section (submerged) is a wet volume housing a suite of science sensors.

- The AUV continues flight in the stratified water for some distance, and then turns an oblique angle to fly back to the upwelling water.
- The AUV repeats the above cycle, thus zigzagging through the frontal zone.
- The AUV mission terminates once the prescribed mission duration has elapsed.

Thus the AUV maps the front in the vertical, cross-front, and along-front dimensions, and tracks it over time.

Figure 5 shows the flow diagram of the algorithm performed on a northward or southward sweep. Front tracking is confined to a bounded region (see Section 2.2). When the AUV reaches any of the bound, it turns around to stay inside the bounds. In the flow diagram, parameters are given values as set in the field experiment (see Section 4).

### 2.2. Front-tracking Bounds

The bounds of the AUV's front-tracking are defined based on prior information of the front's approximate location and orientation, as well as the AUV operational safety considerations. For example, during the Tethys AUV's front-tracking missions in Monterey Bay from May 29 to June 4, 2013 (to be presented in Section 4), the bounds are marked by the dashed lines in Figure 6. A northern

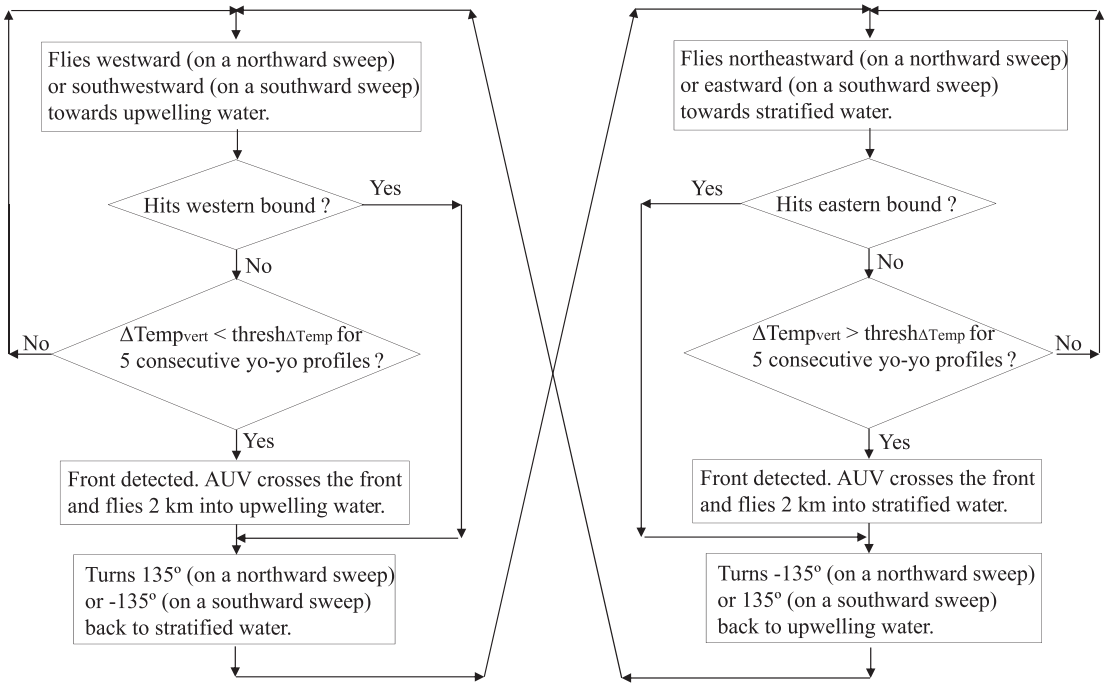


**Figure 5.** Flow diagram of the AUV front-tracking algorithm performed on a northward or southward sweep.

latitude and a southern latitude define the northern and southern bounds, respectively. On a northward-sweeping zigzag, when the AUV reaches the northern bound, the vehicle turns around to start a southward-sweeping zigzag. Conversely, on a southward-sweeping zigzag, when the AUV reaches the southern bound, the vehicle turns around to start a northward-sweeping zigzag.

The eastern bound is set by a certain offshore distance, to keep the AUV at a safe distance away from the shore. The western bound is a line parallel to the front's typical orientation (learned from historical satellite SST observations), to constrain the AUV's track to stay near the frontal zone. On each single transect on the zigzag track, if the AUV reaches the western or eastern bound without detecting the front, the vehicle will make a turn onto the next transect that brings the vehicle back into the bounding box.

## 3. TETHYS AUV

The Tethys long-range AUV (Bellingham et al., 2010b), shown in Figure 4, is 2.3 m long and 0.3 m (i.e., 12 in.) in diameter at the midsection. The propeller-driven vehicle can run effectively from 0.5 to 1 m/s. Using a primary battery, the AUV has demonstrated a range of 1800 km (in three weeks) at a speed of 1 m/s. By adopting power-saving strategies, the vehicle is expected to achieve ranges in excess of 3,000 km (Hobson et al., 2012). Long range is achieved by minimizing propulsion power consumption through a careful design of a low-drag body and a high-efficiency propulsion system. In addition, by using a buoyancy engine, the vehicle is capable of ballasting to neutral buoyancy and drifting in a lower power mode. The Tethys AUV thus combines the merits of propeller-driven and buoyancy-driven vehicles. The vehicle's sensor suite includes Neil Brown temperature and conductivity sensors, a Keller depth sensor, a WET Labs ECO-Triplet Puck fluorescence/backscatter sensor, an Aanderaa dissolved oxygen sensor, an In Situ Ultraviolet Spectrophotometer (ISUS) nitrate sensor, and a LinkQuest Doppler velocity log (DVL) of model NavQuest 600 Micro.

The AUV's underwater navigation is by DVL-aided dead reckoning. When the seabed is within the DVL's bottom-lock range (110 m), the DVL measures the vehicle's velocity relative to the seabed. This velocity vector is rotated into the Earth reference frame using heading and attitude measurements, and then integrated in time to estimate the AUV's location. When the seabed is out of the DVL's bottom-lock range, the vehicle uses the estimated speed (based on the propeller's rotation rate) and the measured heading and attitude to estimate its underwater location. The vehicle periodically ascends to the surface for a global positioning system (GPS) fix to correct the AUV's underwater navigation errors (Bellingham et al., 2010a).

The AUV software architecture uses state-configured layered control (Bellingham & Consi, 1990), which divides the vehicle's operations into a group of behaviors assigned

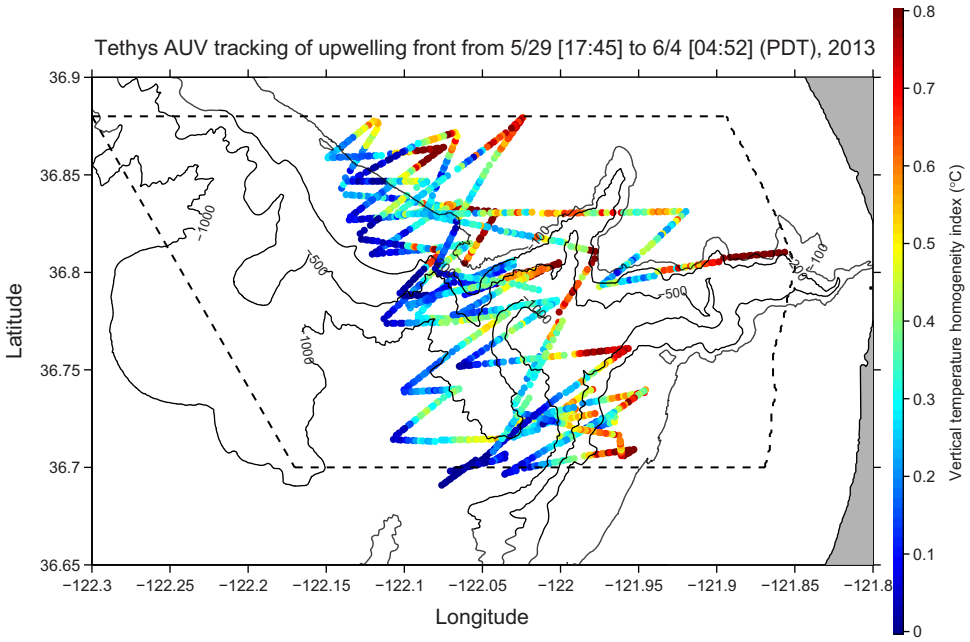


**Figure 6.** From May 29 to June 4, 2013, the Tethys AUV autonomously detected and tracked an upwelling front in Monterey Bay. Color on the AUV's track denotes the value of $\Delta Temp_{vert}$ (i.e., VTHI). The bounds of front-tracking are marked by the dashed lines. See Figure 10 to view each northward or southward sweep.

with different levels of priority. For each AUV mission, the vehicle runs a mission script that invokes appropriate AUV behaviors to achieve a specified goal (Godin, Bellingham, Kieft, & McEwen, 2010; Hobson et al., 2012). Our four-dimensional (4D) front-tracking algorithm is implemented in a mission script by invoking the yo-yo behavior, in which the vehicle's heading is autonomously adapted based on real-time detection of the upwelling front. For front detection, the mission script invokes a behavior for recording temperatures at the participating depths for calculating the VTHI on each yo-yo profile [see Eq. (1)], and the VTHI is directly calculated in real time in the mission script.

## 4. FIELD EXPERIMENT

### 4.1. Overview

In late May 2013, due to a persistent northwesterly wind along the California coastline, intense upwelling developed at the Point Año Nuevo upwelling center, and the upwelling filaments spread southward across the mouth of Monterey Bay. An upwelling front formed between the upwelling filaments across the mouth of the bay and the stratified water inside the bay. From May 29 to June 4, the Tethys AUV ran the presented algorithm to autonomously detect and track the upwelling front, as shown in Figure 6. The AUV flew at a speed of about 1 m/s on a yo-yo trajectory between surface and 50 m depth. During most of the mission, the seabed was out of the DVL's bottom-lock range, so the vehicle used speed estimate and measured heading and attitude to estimate its underwater location, and periodically (about every hour) ascended to the surface to obtain GPS fixes.

The vehicle started on a westward transect from nearshore stratified water toward offshore upwelling water, and it detected a weak front (the front-detection criterion was satisfied but the contrast across the front was weak). The AUV then turned onto a northeastward transect, recrossed the weak front, and turned onto a long westward transect. From this transect on, the vehicle locked onto the main upwelling front and zigzagged through this front, on a northward sweep followed by alternating southward and northward sweeps. The AUV's total 51 front-crossing transects are shown in Figure 6. Color on the AUV's track denotes the value of the vertical temperature homogeneity index $\Delta Temp_{vert}$, which was small in the upwelling water column (on the west side) and large in the stratified water column (on the east side).

### 4.2. Parameter Settings

1. Participating depths for calculating $\Delta Temp_{vert}$ (i.e., VTHI).

   $\Delta Temp_{vert}$ [see Eq. (1)] is the key metric used by the AUV for classifying the water types (stratified water versus upwelling water). Previous temperature measurements in Monterey Bay indicated that the vertical

temperature difference between 5 and 30 m depths provided a strong contrast between upwelling and stratified water columns. So we set the participating depths to 5, 10, 20, and 30 m for the AUV to calculate $\Delta Temp_{vert}$.

2. Front-detection threshold $thresh_{\Delta Temp}$.

   On each yo-yo profile, the AUV compares the calculated $\Delta Temp_{vert}$ and a preset threshold $thresh_{\Delta Temp}$, and accordingly classifies the water column. According to the classification theory (Fukunaga, 1990; Van Trees, 1968), setting the threshold to the middle level between two classes minimizes the total cost of misclassification. Therefore, we set $thresh_{\Delta Temp}$ to a value near the middle level between the two distinct water columns. If $thresh_{\Delta Temp}$ is set too high or too low, the detected front line will be skewed to one side and the AUV's flight coverage will be excessive in one water column but insufficient in the other. Based on temperature data from previous AUV missions in Monterey Bay, we set $thresh_{\Delta Temp} = 0.3\,^{\circ}\mathrm{C}$.

3. Oblique angle of the zigzag track.

   We desire the AUV to zigzag through the front at a close-to-normal angle, because if the AUV's heading were at a small angle to the front (or even parallel to it), the vehicle would easily lose track of the front. Historical satellite SST observations show that the spreading direction of the upwelling filaments (originating from the Point Año Nuevo upwelling center) is often south-southeast. Hence for the AUV's zigzag track, we set the oblique turning angle to 135° so that zigzag transects (either east-west or southwest-northeast) can intersect the front at a close-to-normal angle.

4. Bounds of the front-tracking region.

   The bounds of the AUV's front-tracking region are marked by the dashed lines in Figure 6. The northern and southern bounds were set to 36.88°N and 36.7°N, respectively. The eastern bound was set as the contour of 5 km offshore distance, which was far enough from shore for safe AUV operations and also sufficiently eastward of the frontal zone to bound the front-tracking. The western bound was set as a line extending south-southeast at heading 150° from the northwestern corner [36.88°N 122.3°W] of the bounding box. This line was parallel to the typical south-southeast spreading direction of the upwelling filaments and sufficiently distant to the west of the frontal zone. Thus we set the western bound to constrain the AUV's track to stay near the frontal zone.

   If the AUV were to reach the northern/southern bound, it would switch to the next southward/northward sweep. On each eastward or northeastward transect, the AUV periodically (in each control cycle of 0.4 s) calculated its offshore distance to determine whether it had reached the eastern bound. At the start of each westward or southwestward transect, the AUV made a projection of the transect's intersecting point with the western bound, and then periodically (every 0.4 s) checked whether it had reached the western bound. The projection algorithm is derived in Appendix B. If the AUV were to reach the western or eastern bound, it would make a turn onto the next transect (back into the bounding box), regardless of whether the front was detected. The AUV mission duration was set to 48 h. At the end of each 48-h mission, a shore operator issued a restart command to the AUV (via the Iridium satellite) to continue front tracking. The total front-tracking duration was five and one-half days.

### 4.3. AUV Cross-front Transects and Front-tracking Sweeps

A close-up side view of one northeastward transect from the upwelling water (where $\Delta Temp_{vert}$ was small) to the stratified water (where $\Delta Temp_{vert}$ was large) is shown in Figure 7. The span of each yo-yo profile was about 200 m. When $\Delta Temp_{vert}$ rose above $thresh_{\Delta Temp} = 0.3\,^{\circ}\mathrm{C}$ for five consecutive yo-yo profiles, the AUV determined that it had passed the front and entered the stratified water, and accordingly set the front detection flag, as marked by the blue triangle. Thus the front detection came with a delay of four yo-yo profiles. The delay-corrected front location is marked by the red triangle. In all the remaining figures in this paper, only the delay-corrected front locations will be shown. The AUV continued flight into the stratified water for 40 min (about 2 km) to sufficiently cover the frontal zone, and then ascended to the surface to get a GPS fix and transmit some decimated data back to shore via the Iridium satellite (for monitoring purposes). The next transect was westward (at a $-135^{\circ}$ turn from the northeastward transect shown) for flying back to the upwelling water column. Figure 7 shows that in the stratified water column (on the east side of the front), high chlorophyll concentration was accompanied by low nitrate concentration in shallow water, indicating phytoplankton growth depleting nitrate as a nutrient. In the upwelling water column (on the west side of the front), all water properties were vertically homogenized by the upwelling process, and nutrients (nitrate) were brought up from deeper water to the surface.

On every transect, the AUV detected the front without touching the eastern or western bound, which demonstrated that the experiment design was well informed and the front-tracking algorithm worked effectively. Perspective views of the AUV's temperature and chlorophyll profiles on a northward sweep and the succeeding southward sweep are shown in Figure 8. The red triangles delineate the front's shape. Thus the AUV mapped and tracked the physical and biological conditions across the upwelling front in four dimensions—vertical, cross-front, along-front, and time.

The northward sweep and the succeeding southward sweep overlapped at two locations, as shown in the left panel of Figure 9. The northern overlap was 37 h apart, and the southern overlap was 43 h apart. Temperature and

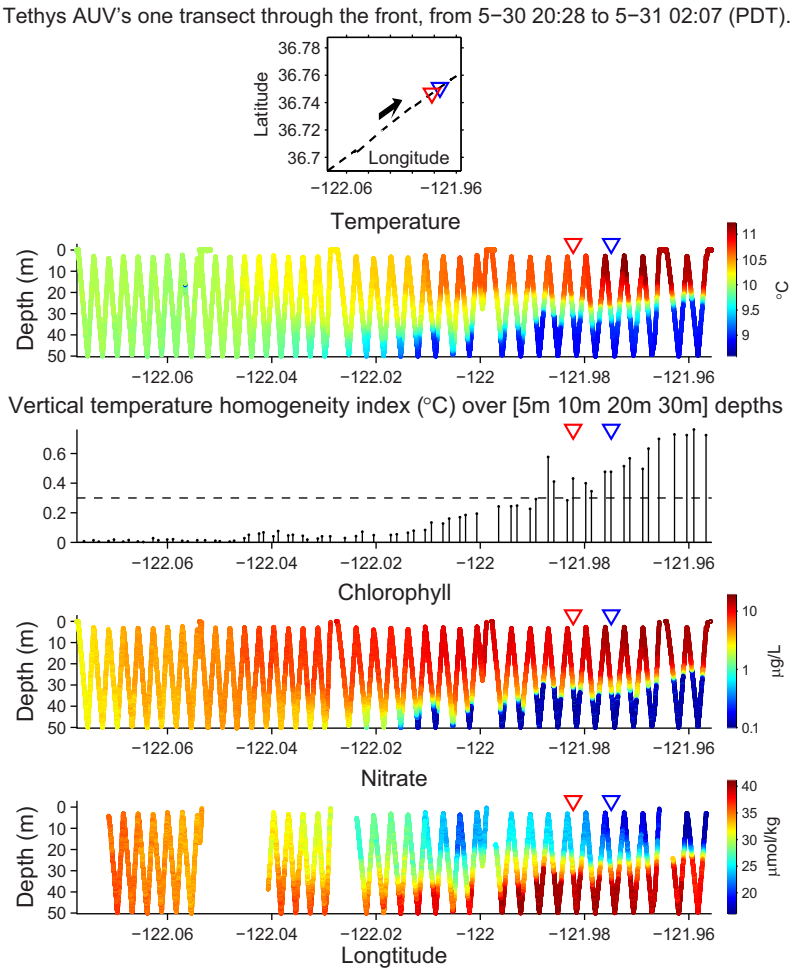


**Figure 7.** First panel: the horizontal track of one AUV transect from upwelling water to stratified water (the vehicle's flight direction is shown by the arrow). Second panel: AUV-measured temperature between surface and 50 m depth. Third panel: $\Delta Temp_{vert}$ (i.e., VTHI) used as the classifier for distinguishing between stratified and upwelling water columns. Fourth and fifth panels: AUV-measured chlorophyll and nitrate between surface and 50 m depth. In each panel, the blue triangle marks the front detection location where the AUV determined that it had passed the front and entered the stratified water column; the red triangle marks the delay-corrected location of the front.

chlorophyll changed considerably over time at the overlap locations. Temperature was less stratified and chlorophyll was much lower on the southward sweep than on the northward sweep, indicating intensified upwelling occurring on the southward sweep. The front was further inshore during the southward sweep, consistent with intensification of upwelling or influx of upwelled water. The noted asymmetry of the northward sweep ("squeezed") and the southward sweep ("stretched') is due to a strong southward current, as will be discussed at the end of this section.

The AUV autonomously tracked the upwelling front for five and one-half days. The shore operators did not intervene other than issuing a restart command at the end of each 48-h AUV mission. The AUV completed four full sweeps plus two partial sweeps, as shown in Figure 10. These AUV transects provided a high-resolution and long-duration depiction of the front.

In Figure 10, small-scale variation of $\Delta Temp_{vert}$ is pronounced on some transects. This means that the clarity of the frontal boundary is variable, and thus supports the methodological aspect of requiring a number of consecutive yo-yo profiles above/below the threshold in determining frontal crossing.

### 4.4. Impact of Strong Current

It is noted that the AUV encountered a strong southward current (up to 0.2 m/s), as shown by the red

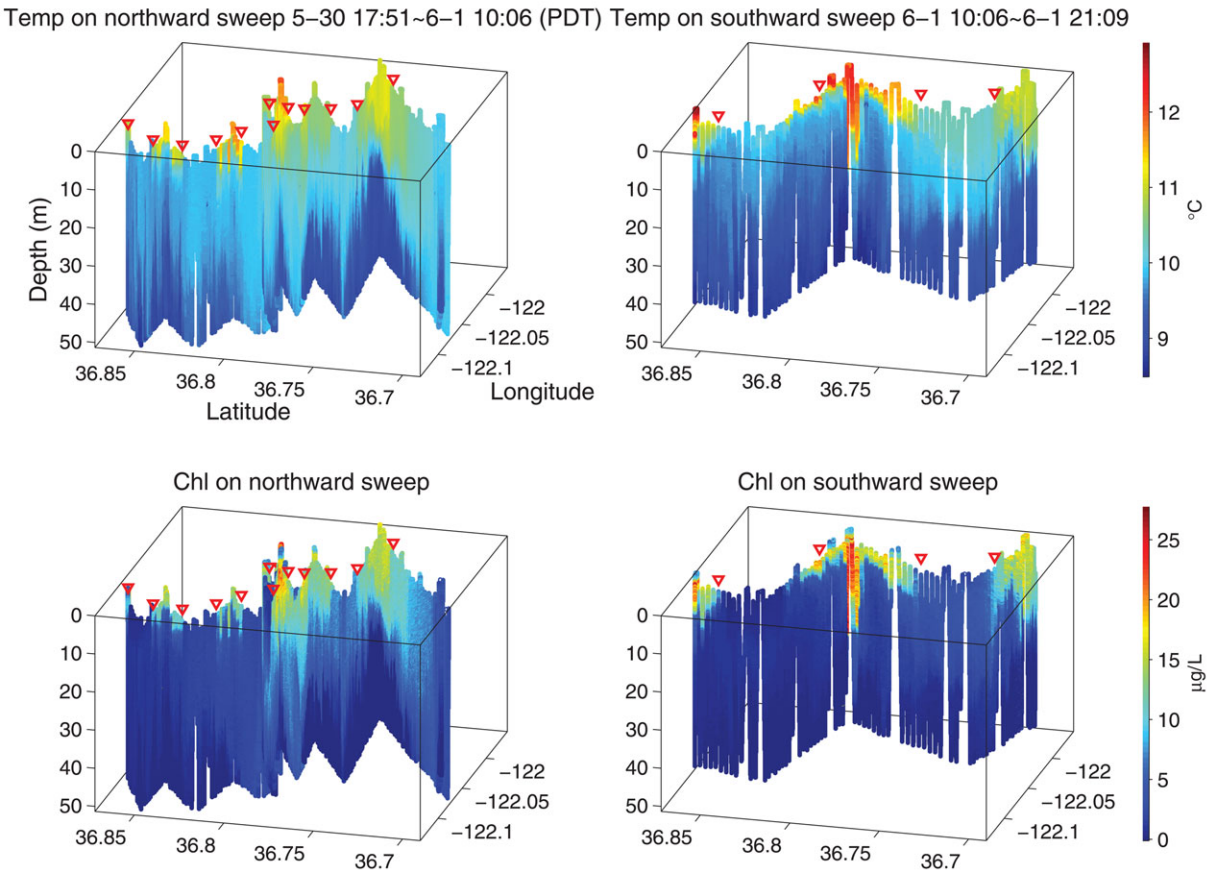


**Figure 8.** Perspective views of the AUV's temperature and chlorophyll profiles on a northward sweep and the succeeding southward sweep. The red triangles mark the front locations.

arrows in Figure 10. The north-south component of current velocity (depth-averaged) is estimated based on how much the AUV's commanded east-west transects were deflected southward (or northward). At the southern tip of the second northward sweep (the third panel in Figure 10), the strong southward current deflected the AUV's supposedly westward transect southward (despite the vehicle's constant westward heading). At the end of this transect, the vehicle ascended to the surface to get a GPS fix and transmit decimated data back to shore. While on the surface, the vehicle was flushed further southward by the current. As a result, the AUV breached the southern bound (36.7°N) before turning onto the succeeding northeastward transect. Subsequently, at the southern tip of the third northward sweep (the fifth panel in Figure 10), the southward current again deflected the AUV's supposedly westward transect southward, causing the vehicle to slightly breach the southern bound.

In the AUV's southward sweeps, the vehicle's flight was assisted by the predominantly southward current, while in the northward sweeps the vehicle flew against the southward current. As a result, the northward and southward sweeps were asymmetric in terms of completion time and front-crossing interval:

1. The AUV's northward sweeps took longer to complete than the southward sweeps.
2. In the northward sweeps, the zigzags were "squeezed" by the opposing current, resulting in dense front crossings. In the southward sweeps, the zigzags were "stretched" by the assisting current, resulting in sparse front crossings.

To reduce the current's impact on AUV front-tracking, an improvement to the algorithm is proposed in Section 5.

## 5. IMPROVEMENTS TO THE ALGORITHM

Based on our experimental experience, we propose the following improvements to the algorithm.

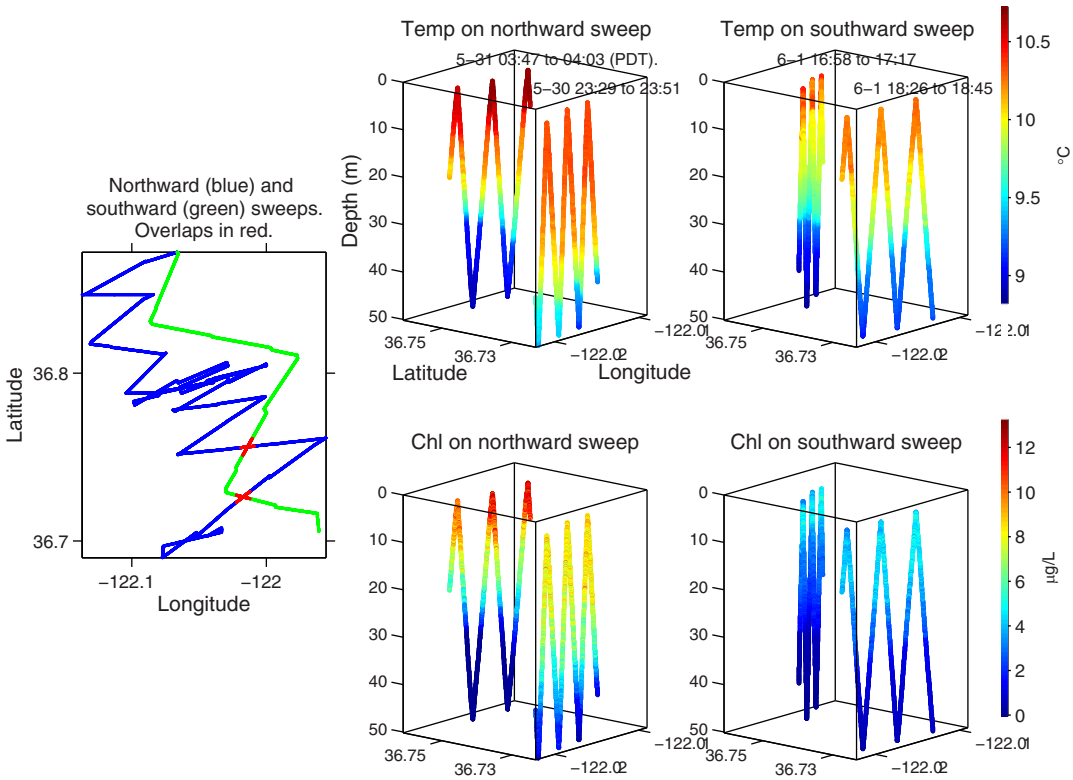


**Figure 9.** Left panel: the AUV's horizontal tracks of the northward sweep (in blue) and the succeeding southward sweep (in green). The segments around the two overlap locations are marked in red. Central and right panels: temperature and chlorophyll profiles on the yo-yo segments around the two overlap locations of the northward and southward sweeps, respectively.

### 5.1. Heading Adjustment for Counteracting the Current

Studying the upwelling front's spatial variation requires a proper sampling interval—the AUV's front crossings should not be too sparse (which causes spatial aliasing) or too dense (which produces redundant information). Keeping a constant front-crossing interval will be helpful for calculating the front's spatial correlation scale and informing future AUV front-tracking designs. To maintain a constant front-crossing interval in northward and southward sweeps, we propose the following scheme to let the AUV adjust its heading to counteract the current. This adjustment will also be beneficial for preventing the current from deflecting the AUV out of the bounding box, as happened in the presented experiment.

The heading adjustment requires estimating the current velocity. If the AUV is equipped with a DVL/ADCP (Doppler velocity log/acoustic Doppler current profiler) and the seabed is within the DVL's bottom-lock range, the Earth-referenced current velocity can be derived from the AUV-referenced current velocity (measured by the ADCP) and the AUV's own Earth-referenced velocity (measured by the DVL). If DVL/ADCP measurements are unavailable, a simpler approach is to estimate the depth-averaged current velocity based on the deviation between the AUV's commanded surfacing location and its actual surfacing location at the end of a yo-yo transect.

Using the estimated current velocity, the AUV applies a heading correction to counteract the current, as illustrated in Figure 11 (assuming a southward current) and explained as follows:

- In southward sweeps, the heading of the eastward transect is adjusted east-northeastward by an angle of $\alpha = arcsin(\frac{v_{current\_south}}{v_{\mathrm{AUV}}})$, where $v_{\mathrm{AUV}}$ is the AUV speed and $v_{current\_south}$ is the southward current speed. For the turn onto the succeeding southwestward transect, the turning angle is increased from $\pi - \beta$ to $\pi - (\beta - 2\alpha)$. Under the southward current, the AUV's actual transects will end up eastward and southeastward, with an included angle close to the desired $\beta$ (the discrepancy will be small when $\alpha$ is small).

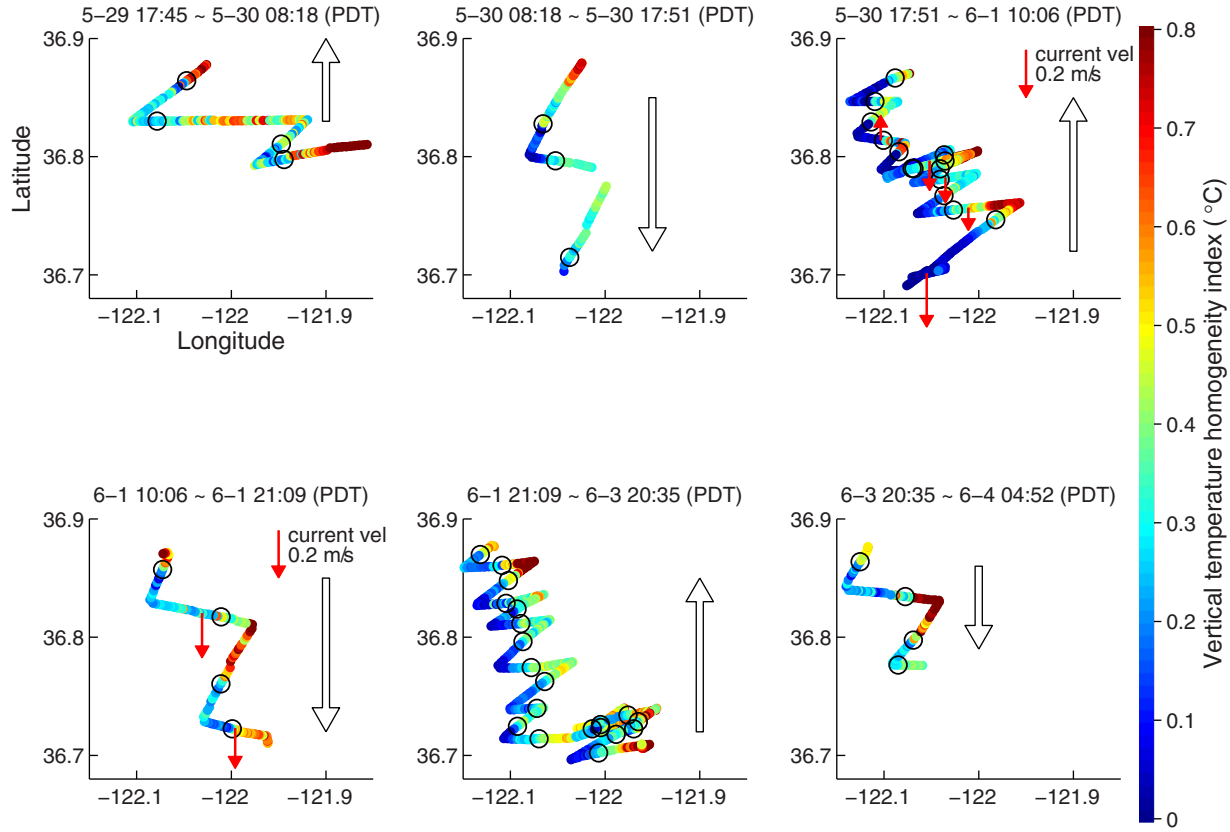


**Figure 10.** The AUV's northward and southward sweeps (the sweep direction is marked by the hollow arrows). Color on the AUV's track denotes the value of $\Delta Temp_{vert}$ (i.e., VTHI). On the third and fourth sweeps, the north-south component of the current velocity is shown by the red arrows. The red arrow in the upper-right corner gives the scale of current velocity. The black circles mark the front locations.

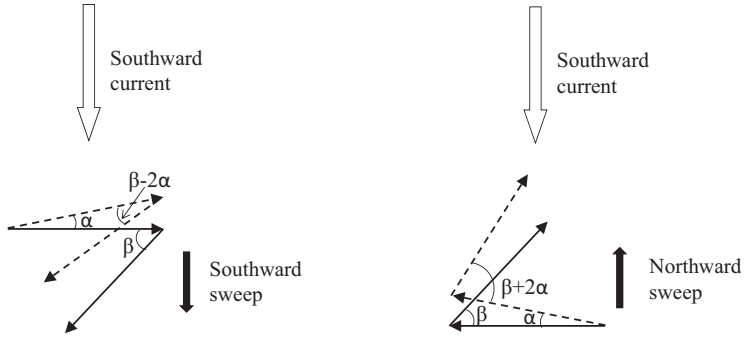


**Figure 11.** Adjustment of AUV transects' headings for counteracting an assumed southward current, on a southward sweep (left panel) and a northward sweep (right panel). The commanded headings are shown by the dashed arrows. The actual transects (under the southward current) are shown by the solid arrows.

- In northward sweeps, the heading of the westward transect is adjusted west-northwestward by an angle of $\alpha$. For the turn onto the succeeding northeastward transect, the turning angle is decreased from $\pi - \beta$ to $\pi - (\beta + 2\alpha)$. Under the southward current, the AUV's actual transects will end up westward and northeastward, with an included angle close to $\beta$.

### 5.2. Adaptive Setting of $thresh_{\Delta Temp}$

As shown in the third panel of Figure 7, the 0.3 °C dashed line (i.e., $thresh_{\Delta Temp}$) lied at just about the middle level between the upwelling water column and the stratified water column. So the setting of $thresh_{\Delta Temp}$ was appropriate in this experiment. The proper setting was due to our prior knowledge of the water columns acquired from previous AUV missions in this region. If we deploy an AUV in an unfamiliar coastal region to detect and track upwelling fronts, it is desirable to enable the vehicle to adaptively set $thresh_{\Delta Temp}$, through the following steps:

1. Deploy the AUV near locations where upwelling fronts are likely to form, based on information from satellite SST images or previous ship surveys.
2. The AUV runs a number of long transects (back and forth) perpendicular to the anticipated front orientation, aiming to cover a sufficient distance in both water columns. On each transect, the AUV calculates VTHI on each yo-yo profile and calculates VTHI's variation over the whole transect.
3. If the AUV sees a sharp rise (or drop) of VTHI over the transect, it determines that an upwelling front is detected. The AUV identifies VTHI's high level (in the stratified water column) and low level (in the upwelling water column), and accordingly sets $thresh_{\Delta Temp}$ to their average (i.e., the middle level).
4. With $thresh_{\Delta Temp}$ set, the AUV commences on a 4D front-tracking mission as described in this paper.

information and *in situ* measurements are utilized for setting appropriate values to the thresholds. For example, in this paper, $thresh_{\Delta Temp}$ was preset based on previous AUV survey data. In unsurveyed regions, however, it is desired that the AUV is able to learn the water columns on the fly and adaptively set the threshold (as proposed in Section 5.2). *In situ* learning strategies help us to replace preset thresholds with adaptive decision making [see our other work (Zhang et al., 2010)], enhancing the effectiveness of autonomy in ocean research.

Multi-AUV coordination or collaboration was used in investigating tidal fronts (Bellingham, 1997), ocean fields around a coastal upwelling center (Fiorelli et al., 2006; Leonard et al., 2010), internal waves (Petillo & Schmidt, 2014), and joint estimation and pursuit of dynamic ocean features (Reed & Hover, 2014). In the context of this paper, we suggest a simple scheme of using multiple AUVs to improve the temporal resolution of front tracking. As shown in Figure 10, it took the single AUV more than two days to complete one full cycle of northward and southward sweeps between 36.7°N and 36.88°N. The upwelling front's movement over two days was significant. To capture the front's movement with a finer temporal resolution, we can deploy two AUVs, with one vehicle tracking the front between 36.7°N and 36.79°N and the other vehicle tracking the front between 36.79°N and 36.88°N. In this way, the two AUVs can complete the sweep cycle in half the time required using a single AUV, so as to generate the front's pictures closer to snapshots.

## 6. CONCLUSION AND DISCUSSION

We have developed a method for an AUV to autonomously detect, map, and track an upwelling front in four dimensions. The Tethys long-range AUV demonstrated this method through a 5.5-day front-tracking in Monterey Bay and effectively revealed the spatial (both cross-front and along-front) and temporal variabilities of the upwelling front.

The key to developing successful AUV algorithms is combining oceanographic insight with the AUV's flexible behaviors. In our case, oceanographic insight pointed to the vertical temperature structure as the distinct feature for classifying upwelling and stratified water columns. The front-detection problem was thus simplified to calculating a simple metric, the VTHI, and comparing it with a threshold $thresh_{\Delta Temp}$. The AUV's yo-yo behavior suits real-time calculation of VTHI on each yo-yo profile, and the vehicle's readiness to change heading makes zigzag front-tracking realizable.

In autonomous classification algorithms, threshold setting is unavoidable. Choosing the right threshold level is done to minimize the total cost of misclassification. Prior

## ACKNOWLEDGMENTS

This work was supported by the David and Lucile Packard Foundation. The authors thank Thomas Hoover, Brett Hobson, Michael Godin, Robert McEwen, Denis Klimov, and Ed Mellinger for helping with the Tethys AUV operations. Special thanks to Michael Godin who programmed the initial AUV mission script for fixed-latitude front tracking and subsequently assisted the authors in modifying the mission script for zigzag front tracking. The June climatology of SST and sea surface chlorophyll in Figure 1 was calculated using MODIS (Moderate Resolution Imaging Spectroradiometer) data from the NASA LAADS system, and MODIS data processing was enabled by the NASA SeaDAS software. Synoptic SST images in Figure 2 were obtained from the NOAA CoastWatch all surface temperature image archive (http://coastwatch.pfeg.noaa.gov/erddap). The authors also thank Robert McEwen and Julio Harvey for the helpful discussions on designing the zigzag front-tracking algorithm, and Mariah Salisbury for the help producing Figure 1. The authors appreciate the valuable comments and suggestions from the three anonymous reviewers, which helped to improve the paper.

## APPENDIX A: INDEX TO MULTIMEDIA EXTENSION

| Extension | Media Type | Description |
|---|---|---|
| 1 | Movie | The AUV transects' progression over time |

## APPENDIX B: AUV'S ALGORITHM FOR PROJECTING ITS TRANSECT'S INTERSECTING POINT WITH AN INCLINED BOUND

In the AUV front-tracking experiment presented in Section 4, the western bound was a line extending south-southeast at heading 150° from the northwestern corner [36.88°N 122.3°W] (see Figure 6), rather than a straight bound of a fixed longitude. This required us to develop a fast algorithm for the AUV to judge whether it has reached the inclined bound.

At the start of each southwestward transect (on a southward sweep) or westward transect (on a northward sweep), the AUV made a projection of the transect's intersecting point with the western bound, as illustrated in Figure B1, and then periodically checked whether it had reached the bound.

We use the following notations for the Cartesian coordinates, and the latitude and longitude of three key locations:

- The starting point of the AUV's southwestward or westward transect: $(x_s, y_s)$, $(lat_s, lon_s)$.
- The northwestern corner of the bounding box: $(x_{nw}, y_{nw})$, $(lat_{nw}, lon_{nw})$.
- The AUV transect's intersecting point with the western bound: $(x_b, y_b)$, $(lat_b, lon_b)$.

The goal of projection is to find $(lat_b, lon_b)$ based on $(lat_s, lon_s)$ and $(lat_{nw}, lon_{nw})$. In the left panel in Figure B1 (for a southward sweep), the imaginary westward extension of the eastward transect intersects with the western bound at $(x_0, y_s)$. Trigonometry of the upper triangle gives

$$\frac{y_{nw} - y_s}{x_{nw} - x_0} = -tan(\theta_1) \tag{B1}$$

which reduces to

$$x_0 = \frac{y_{nw} - y_s}{tan(\theta_1)} + x_{nw}. \tag{B2}$$

Trigonometry of the lower triangle gives

$$\frac{y_b - y_s}{x_b - x_0} = -tan(\theta_1), \tag{B3}$$

$$\frac{y_b - y_s}{x_b - x_s} = tan(\theta_2). \tag{B4}$$

Incorporating Equation (B2) into Equations (B3) and (B4) to get rid of $x_0$, we have

$$x_b - x_s = \frac{tan(\theta_1)}{tan(\theta_1) + tan(\theta_2)}(x_{nw} - x_s) + \frac{1}{tan(\theta_1) + tan(\theta_2)}(y_{nw} - y_s), \tag{B5}$$

$$y_b - y_s = \frac{tan(\theta_1)tan(\theta_2)}{tan(\theta_1) + tan(\theta_2)}(x_{nw} - x_s) + \frac{tan(\theta_2)}{tan(\theta_1) + tan(\theta_2)}(y_{nw} - y_s). \tag{B6}$$

Distance ratios in the Cartesian coordinate system can be transformed to ratios of latitude and longitude differences as follows:

$$\frac{x_{nw} - x_s}{x_b - x_s} = \frac{Lon_{nw} - Lon_s}{Lon_b - Lon_s}, \tag{B7}$$

$$\frac{y_{nw} - y_s}{x_b - x_s} = \frac{Lat_{nw} - Lat_s}{cos(\phi)(Lon_b - Lon_s)}, \tag{B8}$$

$$\frac{x_{nw} - x_s}{y_b - y_s} = \frac{cos(\phi)(Lon_{nw} - Lon_s)}{Lat_b - Lat_s}, \tag{B9}$$

$$\frac{y_{nw} - y_s}{y_b - y_s} = \frac{Lat_{nw} - Lat_s}{Lat_b - Lat_s}, \tag{B10}$$

where $\phi$ is the mean latitude of the region, presuming $cos(latitude)$ varies little over the region. For example, in the AUV missions presented in Section 4, latitude range was 36.7°–36.88°, so $cos(latitude)$ ranged from 0.800 to 0.802. Given this small range, it was sufficiently accurate to use a mean latitude $\phi = 36.8°$ with $cos(\phi) = 0.801$.

Incorporating Eqs. (B7), (B8), (B9), and (B10) into Eqs. (B5) and (B6), $Lat_b$ and $Lon_b$ can be expressed in terms of $[Lat_s, Lon_s]$ and $[Lat_{nw}, Lon_{nw}]$:

$$\begin{bmatrix} Lat_b \\ Lon_b \end{bmatrix} = \begin{bmatrix} \frac{tan(\theta_1)}{tan(\theta_1)+tan(\theta_2)} & \frac{tan(\theta_2)}{tan(\theta_1)+tan(\theta_2)} & -\frac{cos(\phi)tan(\theta_1)tan(\theta_2)}{tan(\theta_1)+tan(\theta_2)} & \frac{cos(\phi)tan(\theta_1)tan(\theta_2)}{tan(\theta_1)+tan(\theta_2)} \\ -\frac{1}{cos(\phi)[tan(\theta_1)+tan(\theta_2)]} & \frac{1}{cos(\phi)[tan(\theta_1)+tan(\theta_2)]} & \frac{tan(\theta_2)}{tan(\theta_1)+tan(\theta_2)} & \frac{tan(\theta_1)}{tan(\theta_1)+tan(\theta_2)} \end{bmatrix} \begin{bmatrix} Lat_s \\ Lat_{nw} \\ Lon_s \\ Lon_{nw} \end{bmatrix}. \tag{B11}$$

For a southward sweep (shown in the left panel in Figure B1), incorporating $\phi = 36.8°$, $\theta_1 = 60°$, $\theta_2 = 45°$ into Eq. (B11), we get the projection formula

$$\begin{bmatrix} Lat_b \\ Lon_b \end{bmatrix} = \begin{bmatrix} 0.634 & 0.366 & -0.508 & 0.508 \\ -0.457 & 0.457 & 0.366 & 0.634 \end{bmatrix} \begin{bmatrix} Lat_s \\ Lat_{nw} \\ Lon_s \\ Lon_{nw} \end{bmatrix}. \tag{B12}$$

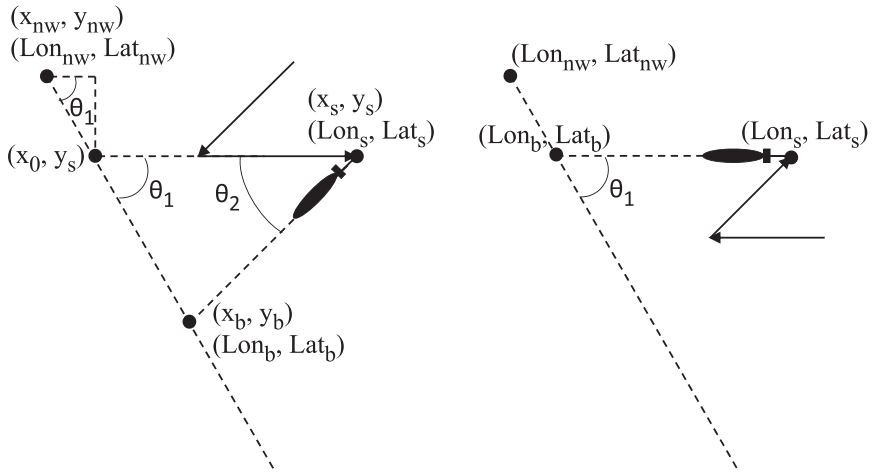


**Figure B1.** Trigonometric relation between the AUV's southwestward/westward transect and the western bound on a southward/northward sweep (left panel: southward sweep, right panel: northward sweep).

For a northward sweep (shown in the right panel in Figure B1), incorporating $\phi = 36.8^\circ$, $\theta_1 = 60^\circ$, $\theta_2 = 0$ into Eq. (B11), we get the projection formula

$$\begin{bmatrix} Lat_b \\ Lon_b \end{bmatrix} = \begin{bmatrix} 1 & 0 & 0 & 0 \\ -0.722 & 0.722 & 0 & 1 \end{bmatrix} \begin{bmatrix} Lat_s \\ Lat_{nw} \\ Lon_s \\ Lon_{nw} \end{bmatrix}. \quad \text{(B13)}$$

In the presented AUV missions, at the start of each southwestward transect (on a southward sweep) or westward transect (on a northward sweep ), the vehicle projected the latitude and longitude of the intersecting point [using Eqs. (B12) or (B13)], and periodically (in every control cycle of 0.4 s) compared its own latitude and longitude $[Lat_{AUV}, Lon_{AUV}]$ with $[Lat_b, Lon_b]$. If $Lat_{AUV} \leq Lat_b$ or $Lon_{AUV} \leq Lon_b$ on a southward sweep (or if $Lon_{AUV} \leq Lon_b$ on a northward sweep), the vehicle would determine that it had reached the western bound.

## REFERENCES


Barber, R., & Smith, R. L. (1981). Coastal upwelling ecosystems. In analysis of marine ecosystems, A.R. Longhurst (ed.) (pp. 31–68). London: Academic Press.

Belkin, I. M., Cornillon, P. C., & Sherman, K. (2009). Fronts in large marine ecosystems. Progress in Oceanography, 81, 223–236.

Belkin, I. M., & O'Reilly, J. E. (2009). An algorithm for oceanic front detection in chlorophyll and SST satellite imagery. Journal of Marine Systems, 78, 319–326.

Bellingham, J. G. (1997). New oceanographic uses of autonomous underwater vehicles. Marine Technology Society Journal, 31(3), 34–47.

Bellingham, J. G., & Consi, T. R. (1990). State configured layered control. In Procedings of the IARP 1st Workshop on Mobile Robots for Subsea Environments (pp. 75–80), Monterey, CA.

Bellingham, J. G., Hobson, B., Godin, M. A., Kieft, B., Erikson, J., McEwen, R., Kecy, C., Zhang, Y., Hoover, T., & Mellinger, E. (2010a). A small, long-range AUV with flexible speed and payload. Ocean Sciences Meeting, Abstract MT15A-14.

Bellingham, J. G., Zhang, Y., Kerwin, J. E., Erikson, J., Hobson, B., Kieft, B., Godin, M., McEwen, R., Hoover, T., Paul, J., Hamilton, A., Franklin, J., & Banka, A. (2010b). Efficient propulsion for the Tethys long-range autonomous underwater vehicle. IEEE AUV 2010 (pp. 1–6).

D'Asaro, E., Lee, C., Rainville, L., Harcourt, R., & Thomas, L. (2011). Enhanced turbulence and energy dissipation at ocean fronts. Science, 332(6027), 318–322.

Fiorelli, E., Leonard, N. E., Bhatta, P., Paley, D. A., Bachmayer, R., & Fratantoni, D. M. (2006). Multi-auv control and adaptive sampling in Monterey Bay. IEEE Journal of Oceanic Engineering, 31(4), 935–948.

Fukunaga, K. (1990). Introduction to statistical pattern recognition, 2nd ed. New York: Academic Press.

Godin, M. A., Bellingham, J. G., Kieft, B., & McEwen, R. (2010). Scripting language for state configured layered control of the Tethys long range autonomous underwater vehicle. Proceedings of the MTS/IEEE Oceans'10 (pp. 1–7).

Harvey, J. B. J., Ryan, J. P., III, R. M., Preston, C. M., Alvarado, N., Scholin, C. A., & Vrijenhoek, R. C. (2012). Robotic sampling, in situ monitoring and molecular detection of marine zooplankton. Journal of Experimental Marine Biology and Ecology, 413, 60–70.

Hobson, B., Bellingham, J. G., Kieft, B., McEwen, R., Godin, M., & Zhang, Y. (2012). Tethys-class long range AUVs - extending the endurance of propeller-driven cruising AUVs from days to weeks. Proceedings of the IEEE AUV'2012 (pp. 1–8).

Jessup, D. A., Miller, M. A., Ryan, J. P., Nevins, H. M., Kerkering, H. A., Mekebri, A., Crane, D. B., Johnson, T. A., & Kudela, R. M. (2009). Mass stranding of marine birds caused by a surfactant-producing red tide. PLoS ONE, 4(2), e4550.

Leonard, N. E., Paley, D. A., Davis, R. E., Fratantoni, D. M., Lekien, F., and Zhang, F. (2010). Coordinated control of an underwater glider fleet in an adaptive ocean sampling field experiment in Monterey Bay. Journal of Field Robotics, 27(6), 718–740.

Petillo, S., & Schmidt, H. (2014). Exploiting adaptive and collaborative auv autonomy for detection and characterization of internal waves. IEEE Journal of Oceanic Engineering, 39(1), 150–164.

Reed, B., & Hover, F. (2014). Oceanographic pursuit: Networked control of multiple vehicles tracking dynamic ocean features. Methods in Oceanography, 10, 21–43.

Ryan, J., Harvey, J. B. J., Zhang, Y., & Woodson, C. B. (2014). Distributions of invertebrate larvae and phytoplankton in a coastal upwelling system retention zone and peripheral front. Journal of Experimental Marine Biology and Ecology, 459, 51–60.

Ryan, J. P., Fischer, A. M., Kudela, R. M., Gower, J. F. R., King, S. A., Marin III, R., & Chavez, F. P. (2009). Influences of upwelling and downwelling winds on red tide bloom dynamics in Monterey Bay, California. Continental Shelf Research, 29, 785–795.

Ryan, J. P., McManus, M. A., Paduan, J. D., & Chavez, F. P. (2008). Phytoplankton thin layers caused by shear in frontal zones of a coastal upwelling system. Marine Ecology Progress Series, 354, 21–34.

Ryan, J. P., McManus, M. A., & Sullivan, J. M. (2010). Interacting physical, chemical and biological forcing of phytoplankton thin-layer variability in Monterey Bay, California. Continental Shelf Research, 30(1), 7–16.

Smith, R. L. (1981). A comparison of the structure and variability of the flow field in three coastal upwelling regions: Oregon, Northwest Africa, and Peru. In Coastal Upwelling, F. A. Richards (ed.) (pp. 107–118). Washington, D.C.: American Geophysical Union.

Ullman, D. S., & Cornillon, P. C. (2000). Evaluation of front detection methods for satellite-derived SST data using in situ observations. Journal of Atmospheric and Oceanic Technology, 17, 1667–1675.

Van Trees, H. L. (1968). Detection, estimation, and modulation theory, Part I. New York: John Wiley and Sons.

Woodson, C. B., Barth, J. A., Cheriton, O. M., McManus, M. A., Ryan, J. P., Washburn, L., & et al. (2011). Observations of internal wave packets propagating along-shelf in northern Monterey Bay. Geophysical Research Letters, 38, L01605.

Woodson, C. B., McManus, M. A., Tyburczy, J. A., Barth, J. A., Washburn, L., Caselle, J. E., Carr, M. H., Malone, D. P., Raimondi, P. T., Menge, B. A., & Palumbi, S. R. (2012). Coastal fronts set recruitment and connectivity patterns across multiple taxa. Limnology and Oceanography, 57, 582–596.

Woodson, C. B., Washburn, L., Barth, J. A., Hoover, D. J., Kirincich, A. R., McManus, M. A., Ryan, J. P., & Tyburczy, J. (2009). Northern Monterey Bay upwelling shadow front: Observations of a coastally and surface-trapped buoyant plume. Journal of Geophysical Research, 114(C12013).

Zhang, Y., Bellingham, J. G., Ryan, J. P., Kieft, B., & Stanway, M. J. (2013). Two-dimensional mapping and tracking of a coastal upwelling front by an autonomous underwater vehicle. Proceedings MTS/IEEE Oceans'13 (pp. 1–4).

Zhang, Y., Godin, M. A., Bellingham, J. G., & Ryan, J. P. (2012a). Using an autonomous underwater vehicle to track a coastal upwelling front. IEEE Journal of Oceanic Engineering, 37(3), 338–347.

Zhang, Y., McEwen, R. S., Ryan, J. P., & Bellingham, J. G. (2010). Design and tests of an adaptive triggering method for capturing peak samples in a thin phytoplankton layer by an autonomous underwater vehicle. IEEE Journal of Oceanic Engineering, 35(4), 785–796.

Zhang, Y., Ryan, J. P., Bellingham, J. G., Harvey, J., McEwen, R. S., Chavez, F., & Scholin, C. (2011). Classification of water masses and targeted sampling of ocean plankton populations by an autonomous underwater vehicle. Abstract OS21A-1609, AGU Fall Meeting.

Zhang, Y., Ryan, J. P., Bellingham, J. G., Harvey, J. B. J., & McEwen, R. S. (2012b). Autonomous detection and sampling of water types and fronts in a coastal upwelling system by an autonomous underwater vehicle. Limnology and Oceanography: Methods, 10, 934–951.

Zhang, Y., Ryan, J. P., Godin, M. A., & Bellingham, J. G. (2012c). Observing coastal upwelling front dynamics by AUV tracking, remote sensing, and mooring measurements. Abstract OS31H-04, AGU Fall Meeting.